Corrosion Science 183 (2021) 109307

Contents lists available at ScienceDirect

Corrosion Science

journal homepage: www.elsevier.com/locate/corsci

Hydrogen enhanced cracking via dynamic formation of grain boundary inside aluminium crystal

De-Gang Xie [a], Liang Wan [b,*], Zhi-Wei Shan [a,*]

[a] Centre for Advancing Materials Performance from the Nanoscale (CAMP-Nano) & Hysitron Applied Research Centre in China (HARCC), State Key Laboratory for Mechanical Behaviour of Materials, Xi'an Jiaotong University, Xi'an, 710049, China
[b] Hubei Key Laboratory of Accoutrement Technique in Fluid Machinery and Power Engineering, School of Power and Mechanical Engineering, Wuhan University, Wuhan, 430072, China

ARTICLE INFO

Keywords:
Hydrogen embrittlement
In situ bending test
Low angle grain boundary
Transgranular cracking
A. Aluminium
B. TEM
B. Modelling studies
C. Hydrogen embrittlement

ABSTRACT

By *in situ* bending tests inside an environmental transmission electron microscope, we found that from the pre-crack tip of single crystalline aluminium cantilevers, dislocations are emitted and self-organized to build a low angle grain boundary (LAGB), along which the crack propagates more easily in hydrogen atmosphere than in vacuum. Atomistic modelling suggests that the LAGB formed can strongly trap hydrogen atoms, and its cohesive strength can be substantially reduced. These results imply that the hydrogen-induced transgranular crack in a polycrystalline metal can proceed by repeating a process of dynamically forming a hydrogenated LAGB and its subsequent separation in grain.

1. Introduction

Hydrogen embrittlement is a pervasive safety concern for almost all industrially-important metals and alloys, and is responsible for many structural failures when the service environment of materials is H-containing, such as oil wells, humid air, sea water, etc. However, despite the enormous efforts in the past century, the mechanistic understanding of hydrogen-induced cracking (HIC) is still on the debate at multiple scales [1–12].

From the fractography perspective, hydrogen embrittled metals often crack in two modes: intergranular and transgranular. For hydrogen-induced intergranular cracking, the cracks propagate well along the pre-existing grain boundaries (GBs) [13,14], indicating that GBs play an important role in hydrogen embrittlement fracture of metals. This can usually be explained by the hydrogen enhanced decohesion (HEDE) theory, which states that gathering of hydrogen atoms in local area of the metals can weaken the metallic bonds there located, thus lead to the decohesion of the material under tensile stress [15,16]. Among typical lattice defects, GB is generally considered as a strong trap for hydrogen atoms, where local H atoms density is usually much higher than in the lattice [17,18]. Meanwhile, dislocation activities can also contribute much to the hydrogen-induced cracking of GBs. For example, some hydrogen-induced intergranular fracture surfaces often come with fine slip traces [14,19], indicating that the cracking of the GB also involves dislocation activities [14]. It was suggested that the reaction of dislocations with GB can activate the GB and largely facilitates the initiation and propagation of the hydrogen-induced intergranular cracks, and it can even make the cracks quasi-cleavage like [12].

The quasi-cleavage feature is more frequently observed in the transgranular-type hydrogen induced cracking. Typical quasi-cleavage fracture surfaces usually show fine river markings or nanovoids/dimples at surface [3,20–22], as a result of intense dislocation activities in a small volume at the crack tip. To explain the quasi-cleavage fracture, the hydrogen enhanced localized plasticity (HELP) theory was proposed [7,23–26] and widely cited [2,3,7,9,27,28]. The HELP theory suggests that hydrogen could promote the dislocation motion [25] or inhibit cross-slip of dislocations [26], which in turn facilitates the localization of plastic deformation and faster fracture within the material [7]. However, the hydrogen effect on individual dislocation behaviour seems to be quite material-dependent, since contradictory evidences exist to reveal quite different effects [6,8,29]. More importantly, it is not clear as to how the behaviour change in individual dislocation can cause localized plasticity, and how the localized plasticity leads to premature cracking.

Some recent works have attempted to bridge the knowledge gap

* Corresponding authors.
E-mail addresses: liangwan@whu.edu.cn (L. Wan), zwshan@mail.xjtu.edu.cn (Z.-W. Shan).

https://doi.org/10.1016/j.corsci.2021.109307
Received 21 October 2020; Received in revised form 11 January 2021; Accepted 5 February 2021
Available online 8 February 2021

between H-modified individual dislocation behaviour and hydrogen induced cracking. These experiments generally reported more refined microstructure units (e.g., dislocation cells, sub-grains divided by dislocation walls) developed in the presence of hydrogen [14,30]. It was also reported that hydrogen can promote the formation of low-energy dislocation nanostructures which then serve as the sites for crack initiation on loading [31]. Besides, by cold rolling of the metal samples to different reduction strains, different dislocation patterns (e.g., dislocation cell walls with different dislocation density distributions) were found to be formed in the materials, and they can make a difference on the subsequent hydrogen embrittlement behavior of these rolled samples [32]. Altogether, it appears that the hydrogen effects on these dislocation cells/sub-grain boundaries should be critical to the understanding of the HIC, yet less studied till now.

In this work, we choose *in situ* environmental transmission electron microscope (TEM) bending tests on pre-notched cantilevers of single crystalline aluminium, to study the hydrogen effect on the evolution of dislocation substructure and the ensuing cracking process. Combined with atomistic modelling and calculation of the hydrogen effect on GB segregation and cohesive strength reduction, our results provide an excellent example to show the evolution of microstructure towards transgranular cracking in the presence of hydrogen.

2. Materials and methods

2.1. Sample preparation

Single crystal aluminium (99.9995 %) disks were cut into 1.5 mm × 2 mm rectangular plates, which were mechanically polished to ~100 μm in thickness and electrochemically thinned to 1~3 μm at one edge. On the thinned edge, cantilever beams were milled by focus ion beam (FIB, FEI Helios NanoLab 600, operating at 30 keV and 32 pA at final milling step) equipped with a scanning electron microscope (SEM), as shown in Fig. 1. For each cantilever, a hump was fabricated at the floating end to maintain stable touch during mechanical tests, and a notch was fabricated at position about 200 nm away from the support. These notches have measured depths ranging from 1/5 to 1/2 of the beam thickness, with fitted radius of curvature of 20–60 nm. To minimize the ion implantation, the incident angle of the Ga beam is small and nearly parallel to the resulted surface during ion milling, thereby resulting in an implantation depth as small as possible. Also, the final milling step usually uses a lower accelerating voltage (5–16 kV) and beam current (18 pA). All the cantilevers contain pre-existing dislocations resulting from FIB milling, with dislocation density estimated to be from 5×10^{13} m^{-2} to 1×10^{14} m^{-2}. These dislocations are in a state of being pinned by defects like other dislocations and point defects near the surface.

2.2. In situ bending tests in environmental TEM

The bending tests and *in situ* observation of the sample deformation were conducted in an environmental TEM (Hitachi H9500, operating at 300 kV and 2 mA–4 mA emission current). As shown in Fig. 1, three different gas conditions were applied in the bending tests: (1) vacuum, (2) mixed gas of 0.5 Pa Hydrogen and 1.5 Pa Nitrogen, and (3) 2–3 Pa pure Hydrogen. Before the bending test in the hydrogen environment, the samples were immersed in the gaseous atmosphere for at least 30 min, long enough for hydrogen diffusion to reach equilibrium distribution in the samples. The bending tests were performed on Hysitron PI95 H1H PicoIndenter. The cantilever beams were loaded using a diamond tip, which was driven by a MEMS transducer. The displacement and loading force were simultaneously measured by the transducer with force resolution of ~500 nN and the displacement resolution of ~2 nm. All bending tests were carried out using a displacement control mode with the loading rate set at 2~5 nm/s.

2.3. Atomistic modelling and calculation

To support the analysis of experimental results, atomistic modelling and calculation of hydrogen effect on cohesive strength of GBs and segregation effect of hydrogen atoms were performed by using the software package LAMMPS [33]. The angular-dependent interatomic potential for the Al-H system fitted by Apostol and Mishin [34] was adopted. This potential can reproduce a variety of properties for the Al-H system, and was shown to be highly reliable for atomistic simulation of dissolved hydrogen on deformation and fracture of Al [8,34].

Three low angle GBs of $\Sigma243 < 110 > \{11\ 11\ 1\}$ (tilt angle of 7.36°), $\Sigma73 < 110 > \{6\ 6\ 1\}$ (tilt angle of 13.44°), $\Sigma33 < 110 > \{4\ 4\ 1\}$ (tilt angle of 20.05°), and two high angle GBs of $\Sigma5 < 100 > \{3\ 1\ 0\}$ (tilt angle of 36.86°) and $\Sigma21 < 112 > \{1\ 4\ 2\}$ (tilt angle of 44.41°), were selected for the modelling study. To evaluate the hydrogen effect on cohesive strength of GBs in aluminium, the interface cohesive energy model proposed by Rice and Wang [35], which is in line with the elastic-brittle Griffith model and was widely adopted for characterizing the theoretical cohesive strength for GBs [36–39], was employed here. In the Rice-Wang model, the GB cohesive energy is defined to be $2f_s - f_b$, where the f_s and f_b denote excess free energy per unit area for a surface and the GB, respectively [35]. Here we use the 0 K potential energy of the system instead for the calculation. Specifically, small bicrystal models with dimensions equal to a few numbers of coincidence site lattice (CSL) periods of the corresponding GBs were constructed. The three-dimensional periodic boundary condition (PBC) was applied. Hydrogen atoms of different numbers were introduced in the GB zone at the middle of the bicrystal models. For all the bicrystal models, the GB

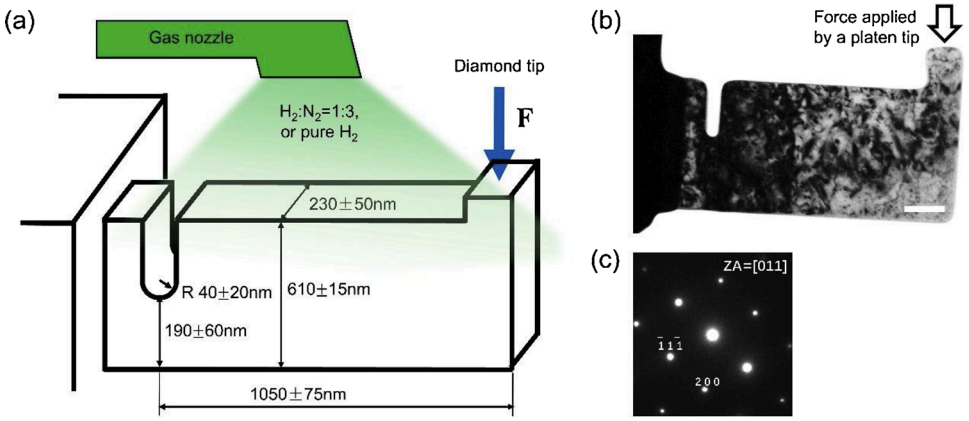

Fig. 1. *In situ* environmental TEM bending test of the notched sample of single crystalline aluminium. (a) Schematic illustration of the sample geometry and dimensions. (b) Bright field TEM image showing the as-prepared cantilever by FIB (scale bar: 200 nm). (c) The corresponding diffraction pattern of the single crystalline aluminium sample.

zone is defined to be a thin slab with thickness of 1.0 nm parallel to the GB plane (i.e., the geometric separation plane of neighbouring grains), and with the GB plane as its middle plane. The hydrogen atoms initially have random distribution in the GB zone. A combination of Metropolis Monte Carlo (MC) [40,41] moves of the hydrogen atoms together with Nose-Hoover molecular dynamics (MD) [42,43] of the bicrystal models at 300 K and zero stress was performed. The hydrogen atoms were confined to move within the GB zone with thickness of 1.0 nm. The models were then subjected to an energy minimization relaxation finally to reach their equilibrium state of GB at 0 K. By separation of the bicrystal models along the middle plane in the GB zone, and using a similar combined procedure, the equilibrium state of the separated surfaces of the GBs at 0 K can be prepared. The cohesive energies of the GBs were calculated by the potential energy difference between the models with and without separated surfaces correspondingly. One can see that we did not consider hydrogen atoms outside the GB zone for calculation of the hydrogen effect on the cohesive strength of GBs. And we assume that the error produced by this simplification is marginal for the calculated values. The cohesive energies of the {1 1 1} lattice plane in Al single crystal with randomly distributed hydrogen atoms of different densities were also calculated in a similar way. The only difference is that, for the separated surfaces of the single crystals with randomly distributed hydrogen atoms, no MD nor MC simulation was performed so as to avoid strong segregation (or mobile effect) of hydrogen atoms on the separated surfaces.

For calculation of the hydrogen atoms segregation ratio of the selected GBs, fairly larger bicrystal models with the dimension perpendicular to the GB plane close to 20.0 nm were prepared. The three-dimensional PBC was applied for these bicrystal models as well. Hydrogen atoms of a bulk concentration of around 10,000~13,000 appm and with a random distribution were introduced into the whole region of models (i.e., no segregation at all initially). MD simulation using the Nose-Hoover dynamics was performed with these bicrystal models at 300 K and zero stress. The overall time of MD simulation adopted for each bicrystal model was 100.0 ns, which is long enough to bring the distribution of hydrogen atoms in the bicrystal models to equilibrium state at 300 K, since the diffusion rate of hydrogen atoms is rather high due to the very low migration barrier of interstitial hydrogen atoms in the face centre cubic (FCC) aluminium lattice (0.19 eV) [34]. By defining the thickness of the GB zone to be 1.0 nm as well, and with appropriate choice of the region of grain interior, the volume density of the hydrogen atoms in both the GB zone and the grain interior can be calculated for each bicrystal model, and their ratio then gives the hydrogen atoms segregation ratio at 300 K correspondingly. It needs to be mentioned that, the hydrogen concentration level in the models here appears to be much higher than that usually reported in experimental study (< 2000 appm) [44,45]. However, since there is a strong segregation effect of hydrogen atoms on the GBs (see results described below), the local hydrogen atoms density on GBs and in grain interior of the models at the bulk hydrogen concentration level here should be comparable to those in practice, consider that the grain size of the bicrystal models here (10.0 nm) is much smaller than that in materials of practice (> 500 nm).

3. Results

3.1. *In situ* bending tests with pre-notched cantilevers in environmental TEM

Fig. 2 shows the results from the *in situ* bending tests with pre-notched cantilevers in environmental TEM. As shown in Fig. 2(a) and (b), the residual bending angle (θ), which is defined by the angle of rotation after unloading, is used as a measure of plastic deformation incurred by the load. During loading, a new crack may nucleate and grow from the notch tip (Fig. 3). For the cantilever samples with different dimensions, the ratio between the new crack length (a) and the initial sample thickness (T_0) measured from the notch tip (Fig. 2(b)) was adopted as a measure to compare the extension of crack growth under certain amounts of loading. The measured values of a/T_0 versus θ for all the tested cantilevers are plotted in Fig. 2(c). The result clearly indicates that in hydrogen-containing environment, all samples exhibit bending-induced growth of new cracks and a/T_0 can reach ~0.5 at bending angle of 20°-40°, while in vacuum, only 2 out of the 11 samples (equivalent to a probability of 18 %) show very limited growth of new cracks.

As to the morphology of the crack tip, we observed that the new crack tip resulted from hydrogen environment test (Fig. 3(c)–(h)) is much longer and sharper than that obtained from vacuum test (Fig. 3(a) and (b)). For most samples tested in vacuum, we only see extended blunting of the notch tip without nucleating a new crack. Therefore, the above results of increased cracking propensity and much sharper crack tip in the hydrogen-containing environment unambiguously demonstrate that under our experimental condition, though only a few Pascal of hydrogen as excited by electron beams of relatively high energy, obvious embrittlement in mode I crack tip of pure aluminium samples can be triggered.

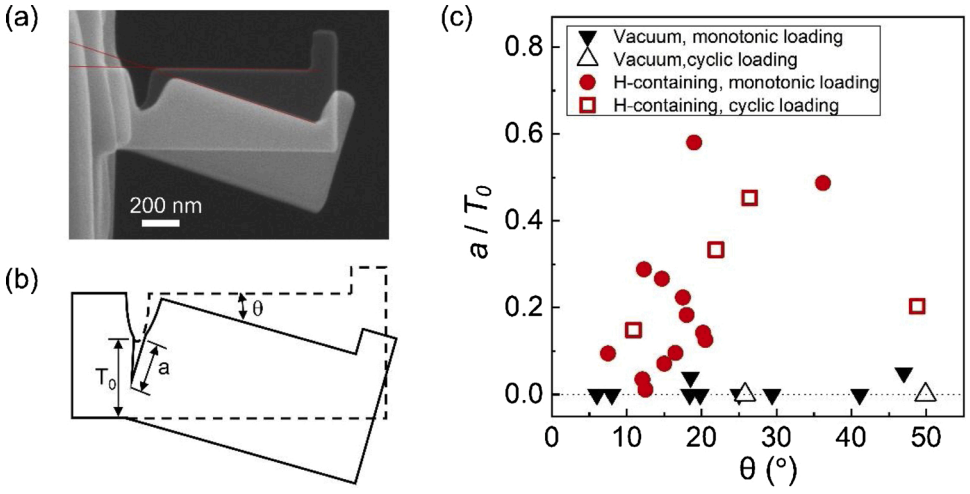

Fig. 2. Cracking propensity during bending deformation of all notched cantilever samples. (a) SEM image of a cantilever sample after bending. A half transparent image of the sample before loading was overlapped on the SEM image for comparison. The red lines were drawn to guide the eyes. (b) Schematic of a cracked sample. (c) Summary of crack propagation distance versus residual bending angle.

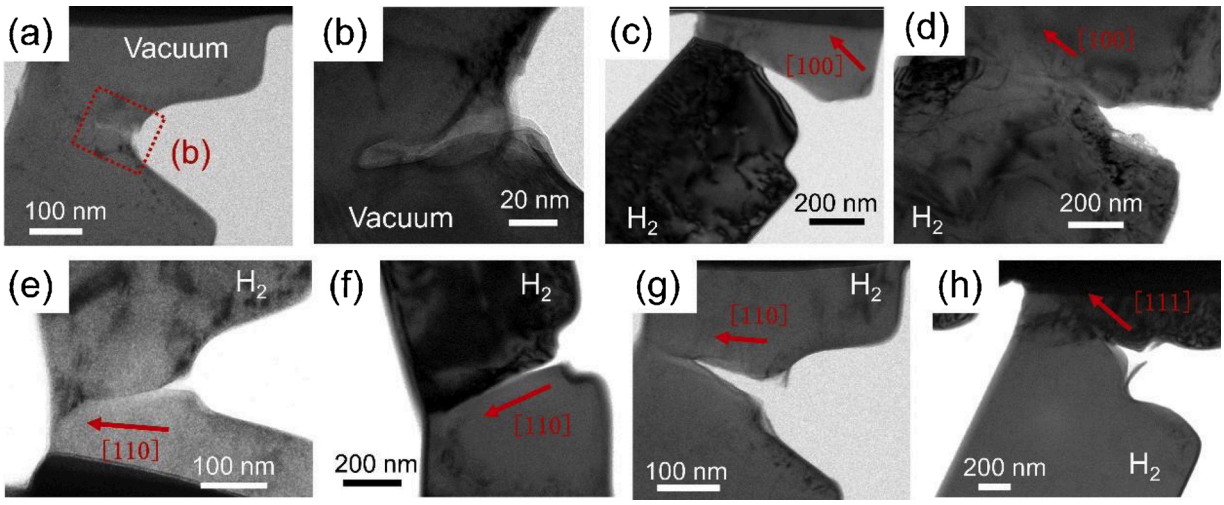

Fig. 3. Cracking morphology of the single crystalline aluminium samples after loading in vacuum ((a) and (b)) and in hydrogen atmosphere ((c)~(h)). Note that a blunt crack tip formed after bending in vacuum ((a) and (b)), while new and sharp cracks formed after bending tests in hydrogen-containing environment ((c)~(h)).

3.2. Microstructure evolution near the crack tips during loading

A typical comparative analysis of the cracking processes is shown in Fig. 4 and Supplementary Movies S1 and S2, which are results from two notched cantilevers of similar geometrical dimensions that were tested in vacuum and in hydrogen, respectively. Three representative snapshots of the cantilevers were extracted from each video at the moments as indicated in Fig. 4(a) and (e). For the cantilever tested in vacuum, Fig. 4(b) and (c) and Supplementary Movie S1 demonstrate that, as the loading force increased, dislocations started to sequentially nucleate at the crack tip at ~1.5 μN, and then moved in a row into the crystal (Fig. 4 (c)) along the direction of the stress gradient. The leading dislocation stopped going further after arriving at the plane of zero stress (neutral plane), and at almost the same moment, the loading force reached the plateau of ~4 μN at displacement of ~100 nm. In the following stage, we saw an increase of dislocation density in the row (Fig. 4(d)), due to more emitted dislocations from the notch tip continuing to be incorporated into the row, accompanied by the blunting of the notch tip without nucleation of a new crack. The formation of these dislocation structures can divide the single crystal sample into several individual grains with

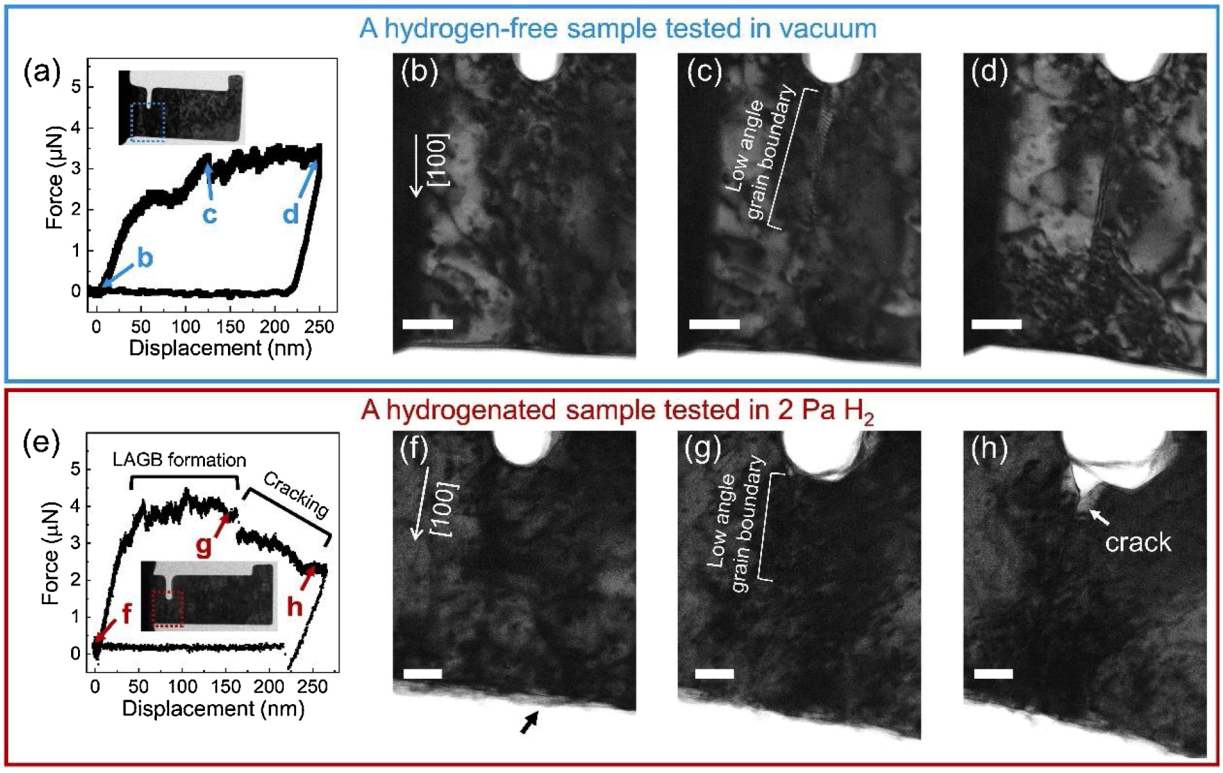

Fig. 4. The evolution of dislocation substructure near the crack tip during the bending tests in vacuum and in hydrogen environment. (a)-(d) are bending results in vacuum and (e)-(h) in hydrogen environment. (a) and (e) are typical force-displacement curves of the notched cantilever. The inserts are bright field TEM images showing the entire cantilever before bending, and the areas boxed with dash lines were recorded as movies. (b)-(d) are snapshots from the movie at the moments as marked in (a) to show the evolution of dislocation configuration at the notch tip, which results in the formation of a LAGB ((c) and (d)). (f)-(h) are snapshots of the bending process as marked in (e), which show the formation of a similar LAGB (g) but also nucleates a new crack in the later stage (h). All scale bars represent 50 nm.

small crystallographic misorientations. As shown in Fig. 5, this crystallographic misorientation can be simultaneously confirmed from the analysis of change of sample morphology, diffraction pattern, and the high-resolution lattice image. Therefore, this dislocation array structure can be regarded as a low angle grain boundary (LAGB).

The results from a test in 2 Pa hydrogen gas (hereafter referred as hydrogen test) are shown in Fig. 4(e)–(h) and Supplementary Movie S2. The black arrow as indicated in Fig. 4(f) shows the formation of tiny blisters on the surface of the sample (see also the Supplementary Movie S2), which is consistent with that reported in our previous work [46], suggesting that the hydrogen atoms have been introduced into the cantilevers for sure. Compared with results from vacuum test, similar phenomenon of forming a LAGB due to emission of dislocations from notch tip has also been observed in the early stage. However, the starting force for dislocation emission from the notch tip is ~2.5 μN, which is higher than that in vacuum test. When the leading dislocation reached the neutral plane, a peak force of ~4 μN also appeared at nearly the same displacement of ~ 100 nm, as can be seen in Fig. 4(e). This peak force is followed by a short stage of plateau, corresponding to the continued increase of dislocation density in the LAGB. To explain the higher activating force for dislocation emission and propagation, we carefully examined the deformation videos, and noticed that some of the pre-existing dislocations in an initial state of being pinned by surface or other local stress centres were also kicked into motion, which can help relaxing the stress and cause softening of the stress-strain curve. However, before reaching the force plateau, much fewer dislocations were activated into motion in hydrogen tests than that in vacuum tests, probably resulting from the hydrogen pinning effect on dislocation motion which is consistent with our previous observations [8]. Such pinning effect can lead to a stiffer stress-strain response at the early stage of deformation and a sustained high stress level during the development of LAGB at the notch tip for the tests in hydrogen. At the later stage of deformation, an obvious distinction is that a sudden drop of loading force occurred for the hydrogen test at displacement of ~150 nm (Fig. 4(e)), but such kind of force drop was never found in vacuum test before unloading (Fig. 4(a)). From Supplementary Movie S2, this force drop can be related to the nucleation of a new crack where the LAGB meets the notch surface. Nearly in all cases, the new crack propagated into the crystal along the LAGB, as illustrated in Fig. 3(c)–(h). These results demonstrate that, despite of similar dynamic formation process of LAGB by emitting dislocations from crack tip on loading, the LAGB formed in hydrogen environment is much more prone to crack than in vacuum.

3.3. Characterization of LAGBs dynamically formed on loading

Fig. 6(a) shows the relationship between the experimentally measured dislocation density in the LAGB dynamically formed on loading and the misorientation angle across the LAGB. Here, the misorientation angle across the LAGB was measured in the way as illustrated in Fig. 5(b) or (c). The dislocation density in the LAGB was obtained from measurement of the fringe periodicity in the TEM image of the LAGB (Fig. 6(b) and (c)). It needs to be mentioned that the contrast in the TEM images of LAGB may assume two different types of appearance made of alternative black and white short lines. Such line patterns can be interpreted as either dislocation lines or Moiré pattern. The method to differentiate between them is that, in a Moiré pattern the white line and the black lines have the same widths, while for dislocation images the widths can be different.

It can be seen that this relationship perfectly matches the theoretical prediction based on the dislocation model of a tilt GB [47] (see the insert in the Fig. 6(a)). As such, these dislocations are geometrically necessary dislocations (GNDs). The density of GNDs is solely determined by the misorientation angle and the length of Burgers' vector [47]. Since the hydrogen effect on the length of Burgers' vector is at the same order as lattice change, which is negligible even in severely H-charged aluminium [45], the measured data points of dislocation density from both the hydrogen tests and vacuum tests are expected to closely adhered to the theoretical line without detectable difference. Therefore, it is reasonable to infer that the hydrogen charging does not result in a different dislocation structure in the LAGB dynamically formed on loading of the aluminium crystal.

3.4. Hydrogen effect on cohesive strength of GBs and the segregation effect of hydrogen atoms on GBs

The hydrogen effect on the cohesive strength of GBs in aluminium was evaluated by atomistic modelling method with high fidelity interatomic potential for the Al-H system. Three symmetric tilt LAGBs with tilt axis of <1 1 0> and tilt angles of 7.36°, 13.44° and 20.05° (Fig. 7(a)–(c)), and two typical high angle GBs of Σ5 < 100 > {3 1 0} (tilt angle of 36.86°, Fig. 7(d)) and Σ21 < 112 > {1 4 2} (tilt angle of 44.41°, Fig. 7(e)), were selected for the modelling study. Fig. 7(a)–(c) show that the LAGBs are composed by a wall of edge dislocations. The density of dislocations within the wall increases with the increase of the tilt angle, which is in good agreement with the experimental observations shown in Fig. 6. It can be seen that the cores of the dislocations become very

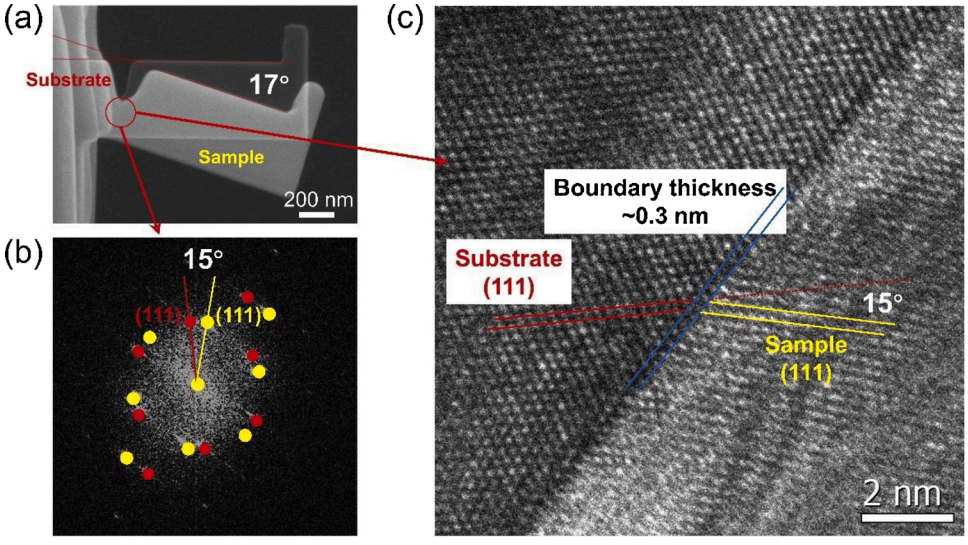

Fig. 5. Misorientation angle across the grain boundary from one typical sample after loading as determined by three different methods: (a) morphology change, (b) diffraction pattern, and (c) high-resolution lattice image.

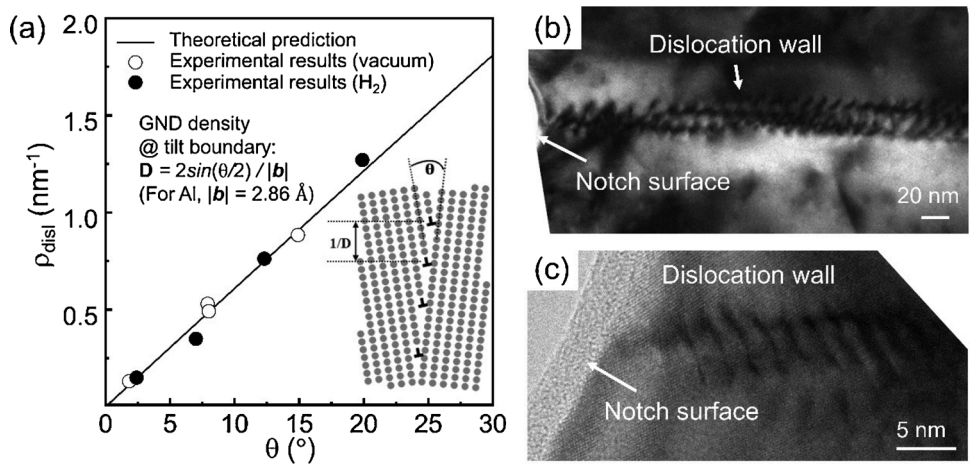

Fig. 6. Characterization of the LAGBs formed in the notched cantilevers after loading. (a) The comparison of the experimentally measured dislocation density in the LAGBs with the theoretical prediction. (b) and (c) are TEM images of the dislocation wall near the notch fronts at low and high magnification, respectively.

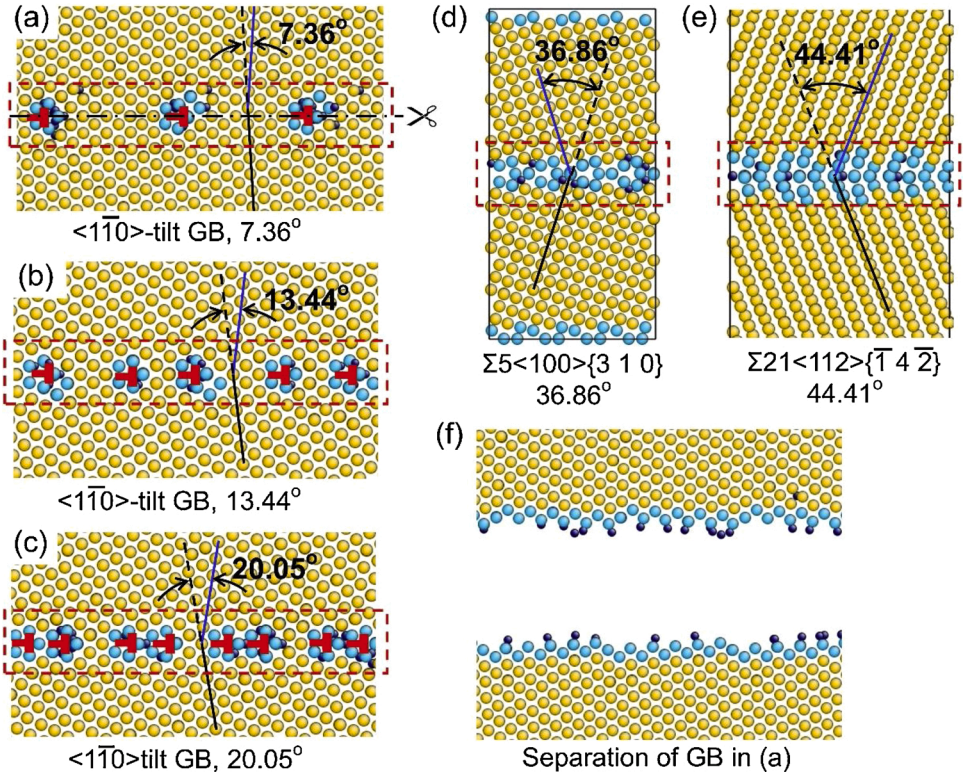

Fig. 7. Atomistic modelling of hydrogen effect on cohesive energy for a few typical grain boundaries in aluminium. (a)-(c) are the atomistic models for three LAGBs in aluminium segregated with H atoms. (d) and (e) are the atomistic models for the high angle GBs of Σ5 < 100 > {3 1 0} and Σ21 < 112 > {1 4 2}, respectively. (f) is the atomistic model for the bicrystal in (a) separated along the GB plane with two surfaces. By using the common neighbour analysis method [61], the aluminium atoms with FCC structure order are represented by yellow spheres, while the non-FCC ones are represented by cyan spheres. The smaller dark blue spheres stand for the H atoms. In (a)-(e), the GB zones defined as the thin slab with thickness of 1.0 nm parallel to the GB plane and with the GB plane as its middle plane for these GBs, are indicated by the dashed rectangles.

close to each other when the misorientation angle is larger than ~20° (Fig. 7(c)). By careful preparation of the equilibrium state of the GBs segregated with different amount of H atoms (see Fig. 7(a)–(e) for example) and the separated surfaces of these GBs (see Fig. 7(f) for example), their cohesive energies can be obtained by adopting the Rice-Wang model [35], and the result is shown in Fig. 8(a). For comparison, the hydrogen-induced reduction of cohesive energy of the {1 1 1} lattice plane which is the highest dense packed plane in aluminium crystal, was calculated as well. It should be noted that the local volume density of hydrogen atoms (i.e., the abscissa of Fig. 8(a)) in the GB was evaluated in the region of GB zone with thickness of 1.0 nm as indicated by the dashed rectangles in Fig. 7, while the same density level of hydrogen atoms of uniform distribution in single crystal lattice was applied for evaluation of the cohesive energies of {1 1 1} lattice plane for proper comparison in Fig. 8(a).

Fig. 8(a) shows that, the cohesive energy of the LAGB (with or without hydrogen atoms) decreases with the increase of the misorientation angle, and it is very close to that of the high angle GBs when the misorientation angle is larger than ~12°. Meanwhile, the cohesive energy level of the high angle GBs is much (10~30 %) lower than that of the {1 1 1} lattice plane (the favoured cleavage plane) of aluminium crystal with the same local volume density of hydrogen atoms. The cohesive energy decreases with the increase of local hydrogen atoms density in the material, which is a clear manifestation of the HEDE effect. In particular, the slope for reduction in cohesive energy by increase of local density of hydrogen atoms is almost twice in the GBs than in the crystal lattice, suggesting that the GBs have much stronger HEDE effect than the crystal lattice for aluminium even without the segregation effect of hydrogen atoms on GBs. In addition, our atomistic modelling and calculation of the segregation effect of hydrogen atoms on GBs shows

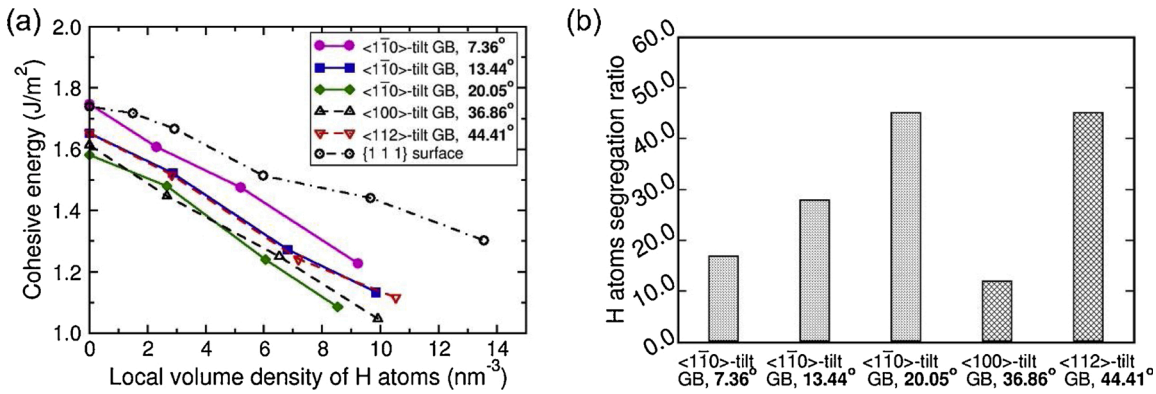

Fig. 8. (a) The calculated cohesive energies (0 K) of the GBs in Fig. 7 segregated with different amount of H atoms. The calculated cohesive energies of the {1 1 1} lattice plane in aluminium crystal with different amount of H atoms are also shown for comparison. Note that the local volume density of H atoms on the GBs is computed as the number of H atoms in the GB zone divided by the volume of the GB zone which is illustrated in Fig. 7. (b) Atomistic modelling and calculated values of hydrogen atoms segregation ratio of the selected GBs in aluminium at 300 K. The tilt angles of the GBs are indicated.

that the hydrogen atoms segregation ratio can range roughly between 10~50 for these GBs at 300 K (see Fig. 8(b)), indicating that hydrogen atoms have high potency to segregate on the GBs in aluminium.

4. Discussion

For metal polycrystals with a relatively large grain sizes (say > 1 μm, which can be applied in our case) and charged with hydrogen atoms of bulk concentration of C_H, and assuming an equilibrium distribution of the hydrogen atoms in the material, the local volume density of hydrogen atoms on the GBs ($\rho_{H/GB}$, in the unit of nm^{-3} here) can be roughly estimated as

$$\rho_{H/GB} = \alpha\, C_H\, \rho_M \quad (1)$$

where ρ_M stands for the atoms number density of the metal matrix in the unit of nm^{-3}, α is the segregation ratio of the hydrogen atoms on the GB, and C_H is defined as the ratio of the number of dissolved hydrogen atoms to the number of atoms in metal matrix. For aluminium with FCC lattice, $\rho_M = 60.2$ nm^{-3} can be obtained. If we take $\alpha = 40$ (Fig. 8(b)), the local volume density of hydrogen atom on the GBs can then be calculated as $\rho_{H/GB} = 2408\, C_H$. In our experiment, here we tentatively assume that the bulk concentration of hydrogen atoms in crack tip region and its surrounding area in the material can reach a value as high as several thousands of appm or even more, as can be reflected from the blisters produced on surface of the samples (Fig. 4(f), see also the Supplementary Movie S2) with hydrogen gas pressure in the bubbles roughly estimated to be around a few hundreds of MPa. Comined with the curves in Fig. 8(a), it can be seen that a large reduction of GB cohesive strength will result upon the formation of the GB at the crack tip on loading. As an example, a bulk concentration of 2000 appm of hydrogen atoms in aluminium can normally produce a local volume density of hydrogen atoms of ~4.8 nm^{-3} on the GB, and it will result in the reduction of the GB cohesive strength of around 20 %, as can be roughly read from the curves in Fig. 8(a). The reduction of the GB cohesive strength scales

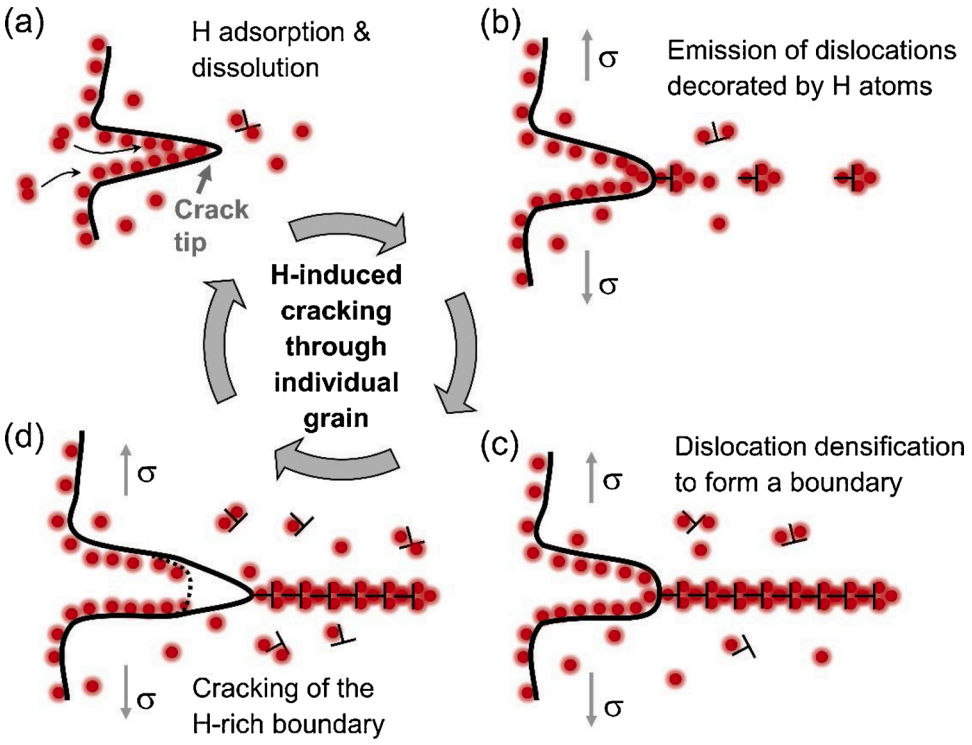

Fig. 9. Schematic illustration of the cracking process in single crystal aluminium on loading. (a) Hydrogen atoms are absorbed at crack-tip surfaces and dissolve in material. (b) Dislocations nucleate from the crack tip surface and hydrogen atoms segregate onto the dislocations. (c) As the dislocations gradually condensed into a dislocation wall, a hydrogen-enriched low angle grain boundary is formed ahead of the crack tip on loading. (d) Crack tip advances along the low angle boundary in a cleavage-like style.

almost linearly as the bulk concentration of the hydrogen atoms in the material increases.

Based on the findings above, we figure out the following four-step physical picture of hydrogen-induced transgranular cracking of an aluminium single crystal, as illustrated in Fig. 9. When exposed in a hydrogen-rich environment, the fresh surface of the crack tip can be saturated with absorbed hydrogen add-atoms, and ingression of hydrogen atoms into the crystal can take place with or without mechanical loading applied, as illustrated in Fig. 9(a). The ingression of hydrogen atoms into the crystal can even be accelerated by irradiation of the electron beam on *in situ* TEM observation of the samples immersed in the hydrogen gas [48]. As a dislocation is nucleated at the stressed crack tip and moves into the crystal interior, the hydrogen atoms, either from the exposed metal surface at crack tip or from the metal interior as the pre-dissolved solutes, can quickly segregate to the dislocation line (Fig. 9 (b)). As more dislocations are emitted from the crack tip and aligned in a row, a LAGB with misorientation linearly proportional to the dislocation density (Fig. 6(a)) will be formed dynamically ahead of the crack tip (Fig. 9(c)). The dislocation density as well as the local hydrogen atoms density in the LAGB can increase to a critical level to induce substantial reduction of boundary cohesion due to the strong HEDE effect in the GBs (Fig. 8(a)). Therefore, cracking can then occur along the hydrogenated LAGB on loading of the material (Fig. 9(d)).

For the role played by hydrogen atoms in the cracking and the mechanism of hydrogen enhanced cracking of the material, our experimental results indicate that, although there is a pinning effect on dislocation motion due to the introduction of the hydrogen in the material, the hydrogen atmosphere does not seem to essentially alter the evolution of dislocation substructures towards dynamically forming of GBs in the aluminium crystal (Figs. 4 and 6). It is therefore reasonable to suggest that the dynamic formation of GBs on loading of the material can serve as a necessary precursory step to trigger the strong HEDE effect of GBs (Fig. 8(a)) for hydrogen enhanced cracking of the single crystal aluminium. Meanwhile, it also needs to be mentioned that, the plasticity in and around the crack tip region may involve many dislocation-GB reactions, which may also facilitate the hydrogen induced cracking, as the reaction can induce atomistic structure distortion to the grain boundary dynamically formed [12].

The fact that hydrogen enhances cracking of the single crystal aluminium via dynamic formation of GBs on mechanical loading sheds light on understanding of the role played by plasticity in hydrogen-induced transgranular cracking of polycrystalline metals in practice. For polycrystalline metals serving in hydrogen environment or pre-charged with hydrogen, cracking of pre-existing GBs can sometimes be suppressed owing to, e.g., insufficient local stress, deficiency of gathering of hydrogen atoms on GB, or lack of dislocation-GB reaction [12]. In such cases, local plasticity within the grain or at crack tip can intensify to develop dislocation substructure, thereby forming LAGBs in interior of individual crystallites by densification and interaction of dislocations in later stages of plastic straining [49]. With segregation of hydrogen atoms on the dynamically formed LAGB, cracking can initiate or propagate along the LAGB facilitated by the strong HEDE effect of GBs, resulting in transgranular fracture of the material. When the crack propagates in this way step-by-step, the blunting and cleavage (Fig. 9) will proceed alternately to produce a quasi-cleavage fracture morphology. In our experiments, the small sizes and the geometry of samples designed here can facilitate a quick emission and arrangement of dislocations within a limited material volume, as well as fast gathering of hydrogen atoms in dislocations from free surface. It turns out that the details of evolution of the dislocation substructure for polycrystalline metals in practice may not be exactly as that revealed by our experiments. Nevertheless, we believe that the LAGBs consisting of a wall of dislocations as found in our experiments should be intrinsically similar to the LAGBs or subgrain boundaries formed near a cracking tip or after severe plastic straining of bulk metals in practice [49]. Therefore, we would like to suggest that the dislocation-mediated local plasticity can serve as a precursory process which is necessary for the formation of LAGBs, and it seems to be the HEDE effect of the GBs that is more important for the initiation or extension of the hydrogen-induced transgranular cracking of the polycrystalline metals in practice.

In the present work, atomistic modelling was employed to calculate the hydrogen effect on reduction of GB cohesive energy as well as the segregation ratio of hydrogen atoms on GBs in the bulk metal of aluminium, which considerably helps the analysis of experimental results. Previously, a handful of atomistic modelling work by using quantum mechanics based first principles calculation methods [1, 50–56] or empirical interatomic potential based methods (such as molecular statics and MD simulation methods) [8,34,57–60] have been performed on investigation of the physics of hydrogen interaction with aluminium. For example, it was reported that the nucleation stress or glide resistance of dislocations can increase upon hydrogen introduction in aluminium crystal [53,54,59], or a pinning effect of the hydrogen Cottrell atmosphere can result [8,60], which are consistent with the *in situ* experimental findings here as described in Section 3.2. A recent first principles calculation of hydrogen effect on cohesive strength of Al-$MgZn_2$ interface reveals the very similar linearly reduction of cohesive energy of interface by increase of the local hydrogen atoms density in the interface zone [56]. On the other hand, a couple of calculations suggest that hydrogen atoms can facilitate the formation of vacancies or vacancy clusters acting as embryos for microvoids and cracks in aluminium [1,55]. And hydrogen induced amorphisation at crack tip of aluminium on loading has also been reported in MD simulation studies [58,59]. Despite the advances made, care must be taken to draw conclusions from the modelling results about the hydrogen embrittlement mechanisms, since there can be inherent limitations in specific modelling methods such as limited size of model or very short duration of physical time simulated or indirect connection between energetics of certain atomistic structure configurations and the physical behaviour of materials under practical conditions. Nevertheless, it is urged that much more efforts are required to be made on using the advanced modelling techniques for in-depth examination of the hydrogen embrittlement behaviour of aluminium and its alloys in the future.

5. Conclusions

In summary, our experimental findings indicate that for the single crystal aluminium exposed to the hydrogen-containing environment, the LAGB which is dynamically formed by emitting dislocations from the crack tip on loading, has a lowered cohesive strength due to the hydrogen enrichment, thus entails a much higher cracking propensity. This is supported by atomistic modelling and calculation which shows that for aluminium, GBs have much stronger HEDE effect than the crystal lattice, as well as a high potency for hydrogen atoms segregation. These results are inspiring for understanding the transgranular cracking of polycrystalline metals in hydrogen environment. In cases where cracking along pre-existing GBs is somehow suppressed, local plasticity realized by dislocation activities in the plastic zone can take place and usually results in the formation of dislocation substructures like LAGBs, which are much more susceptible to cracking after hydrogen enrichment. We propose that the hydrogen enhanced cracking via dynamic formation of GBs can be an important process for the hydrogen embrittlement fracture of metals.

6. Data availability statement

The raw/processed data required to reproduce these findings cannot be shared at this time due to technical or time limitations.

7. Author contributions

Z. S. conceived and designed the project. D.X. conducted the experimental work. L.W. performed the atomistic modelling and

calculation. D.X., and L.W. wrote the paper. All authors contributed to discussions of the results.

Declaration of Competing Interest

The authors declare that they have no known competing financial interests or personal relationships that could have appeared to influence the work reported in this paper.

Acknowledgments

The authors acknowledge supports from the National Key Research and Development Program of China (2017YFB0702001), Natural Science Foundation of China (51971169, 51701151), 111 Project 2.0 (BP2018008), and the Fundamental Research Funds for the Central Universities of China (2042019kf0036, 2042020gf0006). The numerical calculations in this paper have been done on the supercomputing system in the Supercomputing Centre of Wuhan University. We would like to thank Yuanbin Qin, Danli Zhang, Peng Zhang, and Qinqin Fu for assistance in sample preparation using focused ion beam and for help in doing the TEM experiments.

Appendix A. Supplementary data

Supplementary material related to this article can be found, in the online version, at doi:https://doi.org/10.1016/j.corsci.2021.109307.

References

[1] G. Lu, E. Kaxiras, Hydrogen embrittlement of aluminum: the crucial role of vacancies, Phys. Rev. Lett. 94 (2005), 155501.
[2] P. Novak, R. Yuan, B.P. Somerday, P. Sofronis, R.O. Ritchie, A statistical, physical-based, micro-mechanical model of hydrogen-induced intergranular fracture in steel, J. Mech. Phys. Solids 58 (2010) 206–226.
[3] T. Neeraj, R. Srinivasan, J. Li, Hydrogen embrittlement of ferritic steels: observations on deformation microstructure, nanoscale dimples and failure by nanovoiding, Acta Mater. 60 (2012) 5160–5171.
[4] S.P. Lynch, Mechanisms and kinetics of environmentally assisted cracking: current status, issues, and suggestions for further work, Metall. Mater. Trans. A 44 (2013) 1209–1229.
[5] J. Song, W. Curtin, Atomic mechanism and prediction of hydrogen embrittlement in iron, Nat. Mater. 12 (2013) 145–151.
[6] J. Song, W.A. Curtin, Mechanisms of hydrogen-enhanced localized plasticity: an atomistic study using α-Fe as a model system, Acta Mater. 68 (2014) 61–69.
[7] I. Robertson, P. Sofronis, A. Nagao, M.L. Martin, S. Wang, D.W. Gross, K.E. Nygren, Hydrogen embrittlement understood, Metall. Mater. Trans. B 46 (2015) 1085–1103.
[8] D. Xie, S. Li, M. Li, Z. Wang, P. Gumbsch, J. Sun, E. Ma, J. Li, Z. Shan, Hydrogenated vacancies lock dislocations in aluminium, Nat. Commun. 7 (2016) 13341.
[9] O. Barrera, D. Bombac, Y. Chen, T. Daff, E. Galindo-Nava, P. Gong, D. Haley, R. Horton, I. Katzarov, J. Kermode, Understanding and mitigating hydrogen embrittlement of steels: a review of experimental, modelling and design progress from atomistic to continuum, J. Mater. Sci. 53 (2018) 6251–6290.
[10] S. Yin, G. Cheng, T.-H. Chang, G. Richter, Y. Zhu, H. Gao, Hydrogen embrittlement in metallic nanowires, Nat. Commun. 10 (2019) 2004.
[11] R. Shi, Y. Ma, Z. Wang, L. Gao, X.-S. Yang, L. Qiao, X. Pang, Atomic-scale investigation of deep hydrogen trapping in NbC/α-Fe semi-coherent interfaces, Acta Mater. 200 (2020) 686–698.
[12] L. Wan, W.T. Geng, A. Ishii, J.-P. Du, Q. Mei, N. Ishikawa, H. Kimizuka, S. Ogata, Hydrogen embrittlement controlled by reaction of dislocation with grain boundary in alpha-iron, Int. J. Plast. 112 (2019) 206–219.
[13] S. Bechtle, M. Kumar, B.P. Somerday, M.E. Launey, R.O. Ritchie, Grain-boundary engineering markedly reduces susceptibility to intergranular hydrogen embrittlement in metallic materials, Acta Mater. 57 (2009) 4148–4157.
[14] S. Wang, M.L. Martin, P. Sofronis, S. Ohnuki, N. Hashimoto, I.M. Robertson, Hydrogen-induced intergranular failure of iron, Acta Mater. 69 (2014) 275–282.
[15] R. Oriani, A mechanistic theory of hydrogen embrittlement of steels, Berichte der Bunsengesellschaft für physikalische Chemie 76 (1972) 848–857.
[16] R. Oriani, P. Josephic, Testing of the decohesion theory of hydrogen-induced crack propagation, Scr. Metall. 6 (1972) 681–688.
[17] A. Oudriss, J. Creus, J. Bouhattate, E. Conforto, C. Berziou, C. Savall, X. Feaugas, Grain size and grain-boundary effects on diffusion and trapping of hydrogen in pure nickel, Acta Mater. 60 (2012) 6814–6828.
[18] M.A. Mohtadi-Bonab, J.A. Szpunar, S.S. Razavi-Tousi, A comparative study of hydrogen induced cracking behavior in API 5L X60 and X70 pipeline steels, Eng. Fail. Anal. 33 (2013) 163–175.
[19] M.L. Martin, B.P. Somerday, R.O. Ritchie, P. Sofronis, I.M. Robertson, Hydrogen-induced intergranular failure in nickel revisited, Acta Mater. 60 (2012) 2739–2745.
[20] M.L. Martin, J.A. Fenske, G.S. Liu, P. Sofronis, I.M. Robertson, On the formation and nature of quasi-cleavage fracture surfaces in hydrogen embrittled steels, Acta Mater. 59 (2011) 1601–1606.
[21] M.L. Martin, I.M. Robertson, P. Sofronis, Interpreting hydrogen-induced fracture surfaces in terms of deformation processes: a new approach, Acta Mater. 59 (2011) 3680–3687.
[22] A. Shibata, T. Murata, H. Takahashi, T. Matsuoka, N. Tsuji, Characterization of hydrogen-related fracture behavior in As-Quenched low-carbon martensitic steel and tempered medium-carbon martensitic steel, Metall. Mater. Trans. A 46 (2015) 5685–5696.
[23] G. Bond, I. Robertson, H. Birnbaum, On the mechanisms of hydrogen embrittlement of Ni3Al alloys, Acta Metall. 37 (1989) 1407–1413.
[24] T.C. Lee, I.M. Robertson, H.K. Birnbaum, An HVEM in situ deformation study of nickel doped with sulfur, Acta Metall. 37 (1989) 407–415.
[25] H.K. Birnbaum, P. Sofronis, Hydrogen-enhanced localized plasticity - a mechanism for hydrogen-related fracture, Mat. Sci. Eng. A 176 (1994) 191–202.
[26] P.J. Ferreira, I.M. Robertson, H.K. Birnbaum, Hydrogen effects on the character of dislocations in high-purity aluminum, Acta Mater. 47 (1999) 2991–2998.
[27] J.R. Scully, G.A. Young, S.W. Smith, Hydrogen embrittlement of aluminum and aluminum-based alloys, in: R.P. Gangloff, B.P. Somerday (Eds.), Gaseous Hydrogen Embrittlement of Materials in Energy Technologies, Woodhead Publishing Limited, Cambridge, UK, 2012.
[28] Y. Ogawa, D. Birenis, H. Matsunaga, A. Thøgersen, Ø. Prytz, O. Takakuwa, J. Yamabe, Multi-scale observation of hydrogen-induced, localized plastic deformation in fatigue-crack propagation in a pure iron, Scr. Mater. 140 (2017) 13–17.
[29] M. Koyama, S.M. Taheri-Mousavi, H. Yan, J. Kim, B.C. Cameron, S.S. Moeini-Ardakani, J. Li, C.C. Tasan, Origin of micrometer-scale dislocation motion during hydrogen desorption, Sci. Adv. 6 (2020), eaaz1187.
[30] M.L. Martin, P. Sofronis, I.M. Robertson, T. Awane, Y. Murakami, A microstructural based understanding of hydrogen-enhanced fatigue of stainless steels, Int. J. Fatigue 57 (2013) 28–36.
[31] P. Gong, J. Nutter, P. Rivera-Diaz-Del-Castillo, W. Rainforth, Hydrogen embrittlement through the formation of low-energy dislocation nanostructures in nanoprecipitation-strengthened steels, Sci. Adv. 6 (2020), eabb6152.
[32] L. Chen, X. Xiong, X. Tao, Y. Su, L. Qiao, Effect of dislocation cell walls on hydrogen adsorption, hydrogen trapping and hydrogen embrittlement resistance, Corros. Sci. 166 (2020), 108428.
[33] S. Plimpton, Fast parallel algorithms for short-range molecular-dynamics, J. Comput. Phys. 117 (1995) 1–19.
[34] F. Apostol, Y. Mishin, Angular-dependent interatomic potential for the aluminum-hydrogen system, Phys. Rev. B 82 (2010), 144115.
[35] J.R. Rice, J.-S. Wang, Embrittlement of interfaces by solute segregation, Mater. Sci. Eng. A 107 (1989) 23–40.
[36] W.T. Geng, A.J. Freeman, R. Wu, C.B. Geller, J.E. Raynolds, Embrittling and strengthening effects of hydrogen, boron, and phosphorus on a Sigma 5 nickel grain boundary, Phys. Rev. B 60 (1999) 7149–7155.
[37] K.N. Solanki, M.A. Tschopp, M.A. Bhatia, N.R. Rhodes, Atomistic investigation of the role of grain boundary structure on hydrogen segregation and embrittlement in α-Fe, Metall. Mater. Trans. A 44 (2012) 1365–1375.
[38] A.M. Tahir, R. Janisch, A. Hartmaier, Hydrogen embrittlement of a carbon segregated S5(310)[001] symmetrical tilt grain boundary in α-Fe, Mater. Sci. Eng. A 612 (2014) 462–467.
[39] S. Huang, D. Chen, J. Song, D.L. McDowell, T. Zhu, Hydrogen embrittlement of grain boundaries in nickel: an atomistic study, NPJ Comput. Mater. 3 (2017) 1.
[40] N. Metropolis, A.W. Rosenbluth, M.N. Rosenbluth, A.H. Teller, E. Teller, Equation of state calculations by fast computing machines, J. Chem. Phys. 21 (1953) 1087–1092.
[41] D. Frenkel, B. Smit, Understanding Molecular Simulation: From Algorithms to Applications, Elsevier, 2001.
[42] S. Nose, A molecular dynamics method for simulations in the canonical ensemble, Mol. Phys. 52 (1984) 255–268.
[43] W.G. Hoover, Canonical dynamics: equilibrium phase-space distributions, Phys. Rev. A 31 (1985) 1695–1697.
[44] H.K. Birnbaum, C. Buckley, F. Zeides, E. Sirois, P. Rozenak, S. Spooner, J.S. Lin, Hydrogen in aluminum, J. Alloys. Compd. 253–254 (1997) 260–264.
[45] C.E. Buckley, H.K. Birnbaum, Characterization of the charging techniques used to introduce hydrogen in aluminum, J. Alloys. Compd. 330 (2002) 649–653.
[46] D.G. Xie, Z.J. Wang, J. Sun, J. Li, E. Ma, Z.W. Shan, In situ study of the initiation of hydrogen bubbles at the aluminium metal/oxide interface, Nat. Mater. 14 (2015) 899–903.
[47] A.P. Sutton, R.W. Balluffi, A. Sutton, Interfaces in Crystalline Materials, Oxford University Press, Oxford, 1995.
[48] M. Li, D.G. Xie, E. Ma, J. Li, X.X. Zhang, Z.W. Shan, Effect of hydrogen on the integrity of aluminium-oxide interface at elevated temperatures, Nat. Commun. 8 (2017) 14564.
[49] F.J. Humphreys, M. Hatherly, Recrystallization and Related Annealing Phenomena, Elsevier, 2012.
[50] G. Lu, Q. Zhang, N. Kioussis, E. Kaxiras, Hydrogen-enhanced local plasticity in aluminum: an ab initio study, Phys. Rev. Lett. 87 (2001), 095501.
[51] G. Lu, D. Orlikowski, I. Park, O. Politano, E. Kaxiras, Energetics of hydrogen impurities in aluminum and their effect on mechanical properties, Phys. Rev. B 65 (2002), 064102.

[52] C. Wolverton, V. Ozoliņš, M. Asta, Hydrogen in aluminum: first-principles calculations of structure and thermodynamics, Phys. Rev. B 69 (2004), 144109.
[53] R. Zamora, A. Nair, R. Hennig, D. Warner, Ab initio prediction of environmental embrittlement at a crack tip in aluminum, Phys. Rev. B 86 (2012), 060101.
[54] Y. Sun, Q. Peng, G. Lu, Quantum mechanical modeling of hydrogen assisted cracking in aluminum, Phys. Rev. B 88 (2013), 104109.
[55] D. Indeitsev, E. Osipova, The effect of hydrogen on fluctuation embrittlement of aluminum, Tech. Phys. Lett. 45 (2019) 882–885.
[56] T. Tsuru, K. Shimizu, M. Yamaguchi, M. Itakura, K. Ebihara, A. Bendo, K. Matsuda, H. Toda, Hydrogen-accelerated spontaneous microcracking in high-strength aluminium alloys, Sci. Rep. 10 (2020) 1–8.
[57] O. Verners, G. Psofogiannakis, A.C. van Duin, Comparative molecular dynamics study of fcc-Al hydrogen embrittlement, Corros. Sci. 98 (2015) 40–49.
[58] P. White, S.A. Barter, N. Medhekar, Hydrogen induced amorphisation around nanocracks in aluminium, Eng. Fract. Mech. 161 (2016) 40–54.
[59] G.H. Lee, J.S. Shim, C.Y. Cui, H.G. Beom, Hydrogen-induced cracking of an aluminum single crystal: an atomistic simulation, Comput. Mater. Sci. 169 (2019), 109084.
[60] C.D. Spataru, K. Chu, R.B. Sills, X. Zhou, Molecular statics analyses of thermodynamics and kinetics of hydrogen cottrell atmosphere formation around edge dislocations in aluminum, JOM 72 (2020) 3020–3027.
[61] D. Faken, H. Jonsson, Systematic analysis of local atomic structure combined with 3D computer graphics, Comput. Mater. Sci. 2 (1994) 279–286.